Scale-based normalization of spectral data.

Timothy W. Randolph

Department of Biostatistics
University of Washington
Seattle, WA, 98195
206-667-1079
206-667-7998 (fax)
trandolp@u.washington.edu

November 16, 2005

Abstract

Classification of data that arise as signals or images often requires a standardization step so that information extracted from biologically equivalent signals can be quantified for comparison across classes. Differences in global trend, total energy, high-frequency noise and/or local background can arise from variabilities due to instrumentation or conditions during data collection. This article considers some common ways in which such variation is adjusted for and introduces a generalization of the popular "standard normal variate" transformation. Examples from three types of spectroscopy data illustrate the method and its properties.

Keywords: normalization, spectroscopy, preprocessing, standard normal variate, wavelet.

1 Introduction

An increasing number of data types being used in the search for disease markers have the form of spectra, curves or images. These include flow cytometry, liquid chromatography, elastic light fluorescence and a variety of spectroscopies (near infrared (NIR), light scattering, Raman) [7, 9]. Use of these data for classifying disease status typically requires some form of normalization that allows for an effective comparison across a heterogeneous set of samples. Indeed, the data from these highly sensitive instruments can be influenced by subtle changes in settings or conditions and hence are often contaminated by noise, or more precisely, non-discriminatory sample-specific signal ranging from broadband background to high-frequency jitter. In this note we consider some common forms of variability, review some ways in which they are often handled and then introduce an approach that adjusts for both global background and local variabilities. We have in mind data from spectroscopy instrumentations, but the ideas discussed are relevant to signals and images of many types.

The point of normalization is to perform numerically that which was not able to be performed physically during data collection; that is, recover exact replicates when no biological differences exist. Ideally, the sources of non-disease related variation are identified before attempting to adjust for them. Absent this, some exploratory analysis, in addition to careful attention to experimental design, is necessary. In a classical univariate setting one often looks to see how two treatments are manifest in a single individual or unit, thereby allowing one to account for extraneous within-unit variation. Similarly, to determine the within-unit variability in a set of spectra before normalization, an important first step is to create a set of spectra that are nominally replicates (from the same biological sample) but collected under a range of conditions—different collection days, technicians, instrument drift, weather conditions, etc. This seems obvious, but as technology advances and highly-refined instrumentation moves from a role similar to that of the laboratory microscope—where the trained eye of an experienced researcher automatically sifts through uninformative signal—to that of a high-throughput data generator, the temp-

tation is to "shoot first and ask questions later." Indeed, given a wealth of measurements it is tempting to think that sorting out signal from noise should be straightforward. The problem is that when a single datum consists of tens of thousands of correlated values, it is not obvious which parts of its complex structure reflect informative biologically-related signal. And even if one has a reasonable description of this signal, a post-hoc analysis of variance can still be difficult.

In view of this, we consider the problem of normalizing a data set consisting of m spectra, $\{S_i\}_{i=1}^m$, all presumed to contain the exact same biological information, but having been collected from a range of experimental conditions. For convenience we will assume each spectrum is a function of intensity measurements $S(t)$ taken at times (or pixel locations) t in an interval $I = [0, 1]$ (in practice measurements are discretely sampled at t_{k_i}, $k_i = 1, ..., n$, where $I \subset \mathbb{R}^p$). A time-warping alignment or registration of features is sometimes needed so that measurements across spectra ($S_i(t)$ vs. $S_j(t)$, $i \neq j$) can be appropriately compared. We assume this is has been done and focus only on normalization of intensity.

The goal is to transform these nominally equivalent spectra into m exact replicates, $\tilde{S}_i \equiv \tilde{S}$, $i = 1, ..., m$. This problem has infinitely many solutions including some that are useless (such as multiplying each spectrum by zero) and some that are minimally useful (such as transforming each spectrum to a constant; e.g., the grand mean intensity from the entire group). Indeed, a transformation of S_i to $\tilde{S}$ should retain as much information as possible for subsequent use in discrimination between samples. A more reasonable transformation would be to match each spectrum to the mean spectrum, $M(t) := \frac{1}{m}\sum_i S_i(t)$, as in a multiplicative scatter correction [6] which involves a regression of the form $\tilde{S}_i(t) = a_i + b_i M(t)$. However, this may not be helpful in applications where the goal is to normalize a large set of heterogeneous data since even a within-class mean spectrum might be an inappropriate, or at least attenuated, reference spectrum. One aim of this note is to retain an empirical approach that does not depend on matching the spectra to an external reference signal. There is, of course, no universally optimal procedure

for this problem since the answer depends on how the noise enters the data, which varies by platform and implementation.

We begin in Section 2 by establishing notation for several assumptions about how noise versus signal is represented and review some simple methods for normalization. Following this, Section 3 introduces a method that simultaneously extends the most common of these methods, bypasses the need for others (such as smoothing and modeling baseline trends) and incorporates derivative information into the normalization process. Examples involving spectra from three types of instrumentation are presented in Section 4.

2 Common normalizations of spectra

Let S_0 denote a nominal spectrum uncorrupted by noise, and let $\{S_i\}_{i=1}^m$ be the set of replicate spectra, each consisting of some transformation of S_0. The goal is to transform each replicate to a common signal, $S_i \mapsto \tilde{S}_i \equiv \tilde{S}$. Here, $\tilde{S}$ is not necessarily equal to, or even an estimate of, S_0, rather it may be any function that characterizes informative properties common to the data set. The list that follows mathematically describes some obvious ways in which variation enters these data and the methods most commonly used to adjust for them. In practice, some combination of these adjustments would be recommended. A host of articles have studied the effects of these, and other, preprocessing methods for calibration of NIR spectra; see, e.g., [3, 5, 18].

Constant shift. If the replicates exhibit a simple vertical offset between spectra so that $S_i(t) = S_0(t) + c_i$, the goal is met by subtracting a sample-specific constant from each; e.g., $\tilde{S} := S_i - \min_{t\in I}\{S_i(t)\}$, or $\tilde{S} := S_i - \bar{S}_i$, where $\bar{S}_i$ denotes the mean of S_i on I.

Scaling. If each spectrum contains a different amount of energy (variance), large intensities are magnified more than low intensities: $S_i(t) = \eta_i \cdot S_0(t)$. Dividing each spectrum by its total energy $||S||_2 = (\int_I S(t)^2\,dt)^{1/2}$ produces a set of unit-length vectors, $\tilde{S}_i := S_i/||S_i||_2 = S_0/||S_0||_2$. In fact any norm, $||\cdot||$, defined on a vector space containing the spectra will achieve the goal by producing a unit vector in this normed vector space:

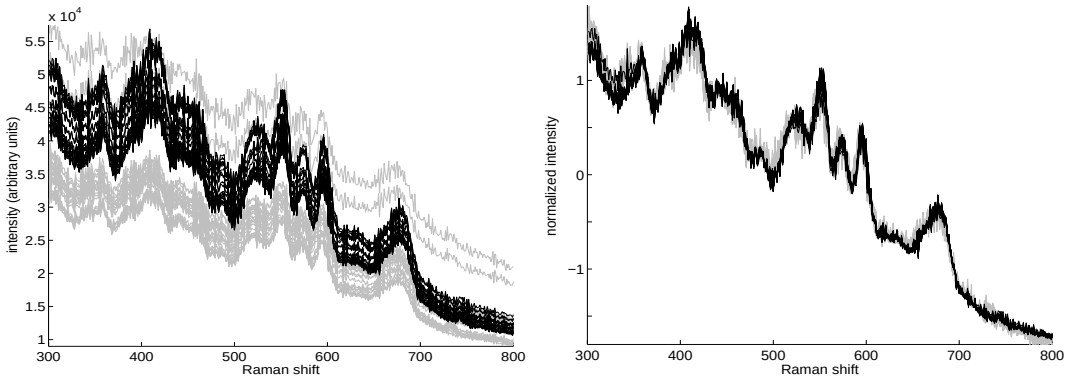

(a) (b)

Figure 1: (a) 50 raw surface-enhanced Raman spectra collected on two days, as indicated by the two colors. (b) The same set of spectra after applying the SNV normalization to each.

$\tilde{S} = S_0/||S_0||$ ($||\tilde{S}|| = 1$).

Standard normal variate. With the goal of both centering (producing mean-zero spectra) and scaling, the popular *standard normal variate* (SNV) transformation was introduced [2] as:

$$\tilde{S}_i(t) := (S_i(t) - \bar{S}_i)/\sqrt{\text{var}(S_i)}. \tag{1}$$

Since $\text{var}(S) \propto ||S - \bar{S}||_2^2$, the transformation (1) is equivalent to a total-energy scaling applied to a centered signal. In [8] this scaling is put in the context of a family of normalization procedures, all of which arise from minimizing the variation of $\tilde{S}_i$ about a mean, the most common being the *multiplicative scatter correction* [6] which takes the form $\tilde{S}_i(t) = (M(t) - a_i)/b_i$.

Figure 1 illustrates a relatively successful application of the SNV transformation to a set of surface-enhanced Raman spectra. These 50 spectra came from the same biological sample collected on two different days [16]. The spectra from the two days (as indicated by color) are biologically identical yet easily distinguished in Figure 1(a) prior to normalization in Figure 1(b).

Baseline correction. A common method of adjusting for a non-constant but low-frequency baseline is to fit a quadratic function (or other polynomial) P_i, to each spectrum and use the difference as the normalized spectrum (e.g., [3]). The assumption in this detrending step is that $S_i(t) = S_0(t) + P_i(t)$, where $P_i(t) = a_i t^2 + b_i t + c_i$, so the adjustment $\tilde{S} := S_i - P_i$ achieves the goal. If a more localized background exists, such as a broad fluorescence bump as may appear in Raman spectra (see, e.g., [19]), a more refined model for P_i would be needed.

Smoothing. If the difference between spectra is known to be a random process, $S_i(t) = S_0(t) + \epsilon_i(t)$, then normalization has the additional complication that any adjustments, $\tilde{S}_i \approx \tilde{S}$, are at best approximate in each case. A variety of smoothing (local-averaging) techniques may be used to obtain a denoised set of essentially equal spectra. The literature on this important topic is vast; for an example of a wavelet-based smoothing method applied to Raman spectra, see [4].

Differentiation. Derivatives of spectra play a useful role in processing spectroscopy signals and algorithms for numerical differentiation are nearly as common as algorithms for smoothing [15, 12]; see [10] for an introductory discussion. Their use can contribute to discrimination, resolution enhancement and detrending. For the latter, note that a quadratic background, P_i, is removed by the second derivative since if $S_i(t) = S_0(t) + P_i(t)$, then $S_i''(t) = S_0''(t)$, so $\tilde{S}_i := S_i''$ achieves the goal. However, numerical differentiation is sensitive to high-frequency noise and without sufficient smoothing the process produces a substantially poorer signal-to-noise ratio than in the original signal. For computation of numerical derivatives, a window is chosen, the width being dependent on several factors: the resolution of the instrument (sampling rate); the derivative being estimated (the second derivative involves a wider window); assumptions about the scale (or width) of informative features; the intensity of the random process noise (a lower signal-to-noise ratio requires a wider window).

3 Scale-based normalization

The global adjustments made by the SNV transformation (the mean and standard deviation) are an attempt to adjust for the fact that features in one signal are offset and magnified versions of those in another. In the case of unequal and nonconstant trends, however, no constant scaling factor will transform one signal into another without first accurately removing these trends. We now introduce a more general and flexible version of the standard normal variates normalization that is less rigidly tied to either the global variance or baseline trend of a spectrum. This scale-based approach is based on locally-defined signal content and includes the SNV normalization as a special case. It allows for greater control over the extraction of localized signal by exploiting a multiscale decomposition of each spectrum. Flexibility is implemented by limiting the scales of content extracted and using only the variance of these portions of the signal. Using all scales coincides with the SNV normalization whereas restricting scales allows one to bypass high-frequency noise, wide-scale background and/or global trend without explicitly modelling any of these. As illustrated by the examples in Section 4, there are several circumstances—i.e., ways in which noise enters the signals—for which a scale-based normalization may be preferable.

3.1 Mulitscale decomposition

Wavelet-based multiscale analysis of spectral data has been used by several authors for background correction [17], noise removal [4] and filtering and feature selection [1]. These approaches are based on the idea that these signals are composed of various scales, or frequency ranges, of information. Moreover, unfolding these scales of content in a time-scale representation facilitates the process of sorting through informative versus uninformative signal. The goal here is similar, but of particular interest is the fact that the variance of a signal is also faithfully decomposed by a wavelet decomposition. For detailed discussions of wavelet analysis see, e.g., the expository article [14] or the comprehensive text [11]. A very brief description of a wavelet decomposition follows.

For convenience, it will be assumed that the domain I of a signal S is an interval

in $\mathbb{R}$ that has been discretely sampled at n "time" points. For this brief discussion, it is assumed that $n = 2^j$, for some integer j, but in practice this is not necessary. The discrete wavelet transform (DWT), denoted here by $\mathcal{W}$, comes from a dyadic subsampling in both time and scale. In time, the dyadic scales roughly correspond to window widths 2^j ($j = 1, ..., \log_2 n$), while for each fixed j a wavelet coefficient function W_j consists of $n/2^j$ values that result from convolving translates of a scale-j wavelet function with S. A similar scaling coefficient function, V_j, results from convolving translates of a scale-j scaling function with S. Properties of the scaling function imply that W_j roughly records local averages in S.

Equally important to this wavelet *analysis* is a *synthesis*. That is, one can form the so-called *detail* functions via $D_j = \mathcal{W}^{-1}(W_j)$, from which the signal S can be recovered. More specifically, S can be decomposed into a ladder of detail functions, D_j, each containing information related to local changes in S occurring on intervals of width 2^j: D_1 is the result of extracting changes in S that occur across a 2^1-unit domain. Writing $A_1 = S - D_1$ expresses the approximation after D_1 is removed. Similarly, changes in S that occur across a 2^j-unit domain lead to a scale-j detail function, D_j. Continuing through J steps results in the decomposition

$$S(t) = A_J(t) + \sum_{j=1}^{J} D_j(t). \tag{2}$$

Figure 2 illustrates the concept with one Raman spectrum and a decomposition into five detail functions, $D_1, ..., D_5$, and the remaining approximation function, A_5. This decomposition was performed using the Haar wavelet family; the inset shows a scale-4 Haar wavelet, its shape helping to emphasize the fact that local differences were extracted. Important properties of this decomposition include the following.

i) The detail functions D_j are mean-zero signals which are, roughly speaking, independent of global background. Moveover, features in the original signal (such as local maxima and inflections) align exactly with events in the detail functions.

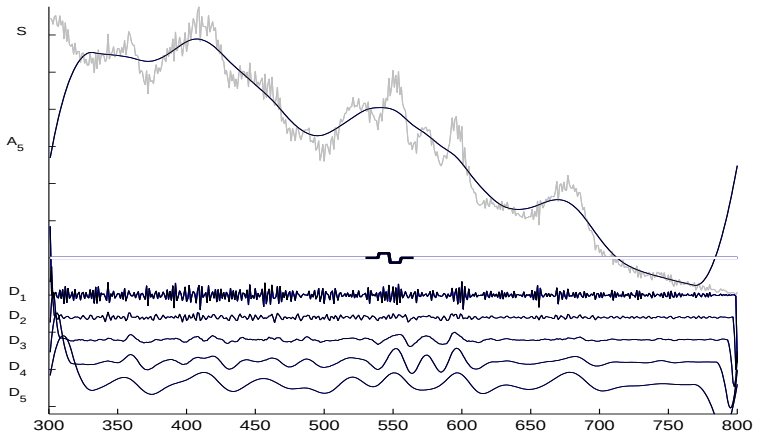

Figure 2: A multiscale decomposition of a noisy version of a Raman spectrum S (gray) using a Haar wavelet; this wavelet function at scale four is shown in the inset. The detail functions, D_1 to D_5 are shown top to bottom, and the scale-5 approximation appears superimposed on S.

ii) A complete decomposition of variance in the signal is preserved by the decomposition:

$$||S||_2^2 = \sum_{j=1}^{J} ||W_j||_2^2 + ||V_J||_2^2 = \sum_{j=1}^{J} ||D_j||_2^2 + ||A_J||_2^2. \tag{3}$$

iii) Using a wavelet having d vanishing moments extracts signal content that is orthogonal to all polynomials of degree less than d: if P is a polynomial of degree less than d and $S = S_0 + P$, then for each j, the wavelet coefficient functions W_j for S and S_0 are equal.

iv) When the wavelet has d vanishing moments, then each scale-j wavelet coefficient function, W_j, is equal to the dth-order derivative of an averaging of S over a domain proportional to the jth scale.

If one uses a portion of the decomposition (4), say $D_k + ... + D_J$, then the analysis of variance in equation (3) allows a SNV-type transformation that restricts attention to these scales of signal content:

$$\tilde{S} = \tilde{S}_{k,J} := \frac{D_k + ... + D_J}{\sqrt{\text{var}(D_k + ... + D_J)}} = \frac{D_k + ... + D_J}{\sqrt{||D_k||_2^2 + ... + ||D_J||_2^2}} \tag{4}$$

A special case of (4) is the SNV normalization (1) which is recovered by using $k = 1$ and $J = \log_2 n$. Indeed, in this case $A_J = \bar{S}$ so the numerator is $D_1 + ... + D_J = S - A_J = S - \bar{S}$, while the denominator is the standard deviation of S. Using $k > 1$ and/or $J < \log_2 n$ generalizes (1) to a normalization based on any specific set of scales. The transformation $S \mapsto \tilde{S}$ defined by (4) will be referred to as a *scale-based normalization* (SBN). The SNV normalization will be denoted by $\tilde{S}_{SNV}$ ($= \tilde{S}_{1,J}$, for $J = \log_2 n$). Useful properties of this normalization result from properties (i)–(iv) of the wavelet decomposition:

a) Interpretation is straightforward since property (i) implies a direct correspondence between features in S and events in $\tilde{S}_{k,J}$.

b) The need to model a global baseline is eliminated. Indeed, each D_i has zero mean and, by property (iii), $\tilde{S}_{k,J}$ is blind to a polynomial background in S when an appropriate choice of wavelet family is used.

c) Restricting k and J to an appropriate subset of scales produces a normalization that is less influenced by either high-frequency noise or broadband variation than SNV. Consequently, local background influences are diminished or removed without modelling them.

d) A consequence of (iv) is that even in the presence of high-frequency noise, $\tilde{S}_{k,J}$ provides a stable extraction of derivative information. In particular, smoothing is not a necessary precursor to extracting first or second derivative information which is an important property when the raw data contains high-frequency noise.

4 Examples of normalizing spectroscopy signals

We consider three different types of spectral signals, the first from a study on the detectability of post-translational modifications in small peptides using surface-enhanced Raman spectroscopy [16]. A second type comes from near infrared spectroscopy. These are inherently smoother, yet apparently have different background properties. In each case, the Daubechies-4 wavelet family (two vanishing moments) was used in producing the

SBN transformations. A third example involves MALDI (matrix assisted laser desorption and ionization) time-of-flight mass spectrometry data where the Haar wavelet family (one vanishing moment) is used.

4.1 Raman spectra

Figure 1 illustrates the SNV normalization applied to a set of surface-enhanced Raman spectra. As a means of illustrating properties of the SBN, a simulated polynomial trend and local background was added to one of these spectra and then processed using SNV and SBN for $k = 4$, $J = 5$. Figure 3(a) shows the two spectra, the simulated background B (the sum of a quadratic polynomial and an exponential), and the result of adding this background to one of these spectra. Figures 3(b) and 3(c) show results of the SNV and SBN transformations, respectively. The SNV normalization is affected by the local background in the region near wavelength 500. The SBN transformations of S_2 and $S_3 = S_2 + B$ are essentially identical and nearly coincide with that of S_1. The primary differences in these occur near the ends of the spectra (wavelengths less than 350 and greater than 750); these are the result of edge effects related to the wavelet transformation.

For reference, we note that the spectra S_1 and S_2 also appear in Figure 1(a), one from each of the two days of data collection (same color coding). The background in Figure 3(a) is of the form $B(t) = a_1t^2+a_2t+a_3+b_1e^{-b_2(t-200)^2}$. Figure 4(a) exhibits the same set of 50 spectra from Figure 1(a) after being perturbed by the addition of 50 different backgrounds, $S_i^B = S_i + B_i$, where each B_i a random perturbation of B, the coefficients a_1, a_2, a_3, b_1 and b_2 chosen from a uniform distribution. Figure 4(b) shows both the SNV and SBN versions of these signals. Of note is the tight agreement shown by SBN for the spectra within each day. On the other hand, there are enhanced differences between these two days near 640 and 740. These differences are apparent to a lesser extent in Figure 1.

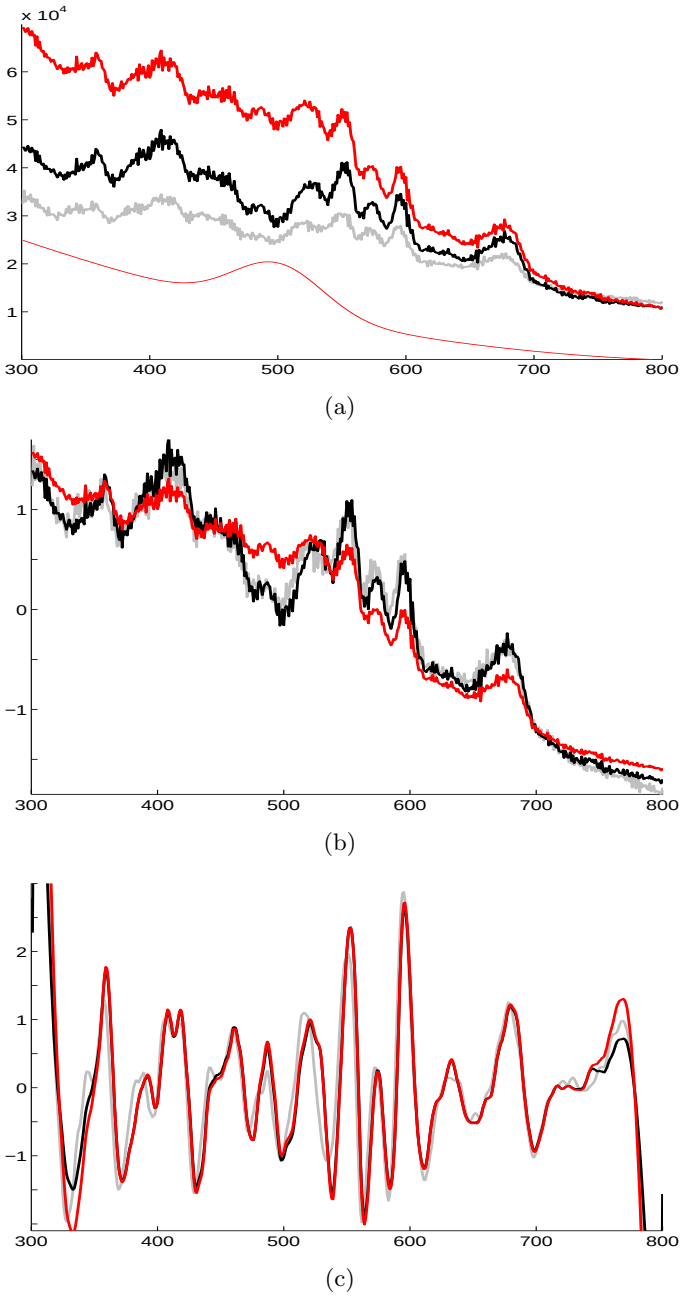

Figure 3: (a) A simulated background B, two Raman spectra S_1 (gray) and S_2 (black), and a modification, $S_3 = S_2 + B$ (red). (b) The same three signals after applying the SNV normalization to each. (c) The transformation of these three signals using SBN with $k = 3,\ J = 5$.

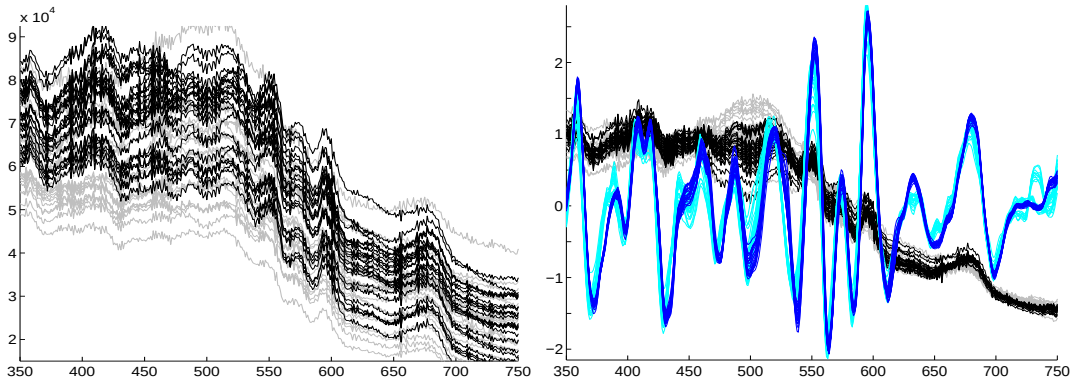

(a) (b)

Figure 4: (a) The 50 Raman spectra from Figure 1(a), each perturbed by the addition of a different background (see text). The gray and black colors indicate the two different collection days. (b) Two normalizations of the spectra in (a): SNV in the background (black and gray) and SBN with $k = 3,\ J = 5$ (dark blue and light blue).

4.2 Near infrared spectra

The next example consists of NIR spectra from pharmaceutical tablets. These come from a published "ShootOut" data set for the 2002 International Diffuse Reflectance Conference.[1] A small random sampling of seven spectra was selected in order to illustrate the flexibility introduced by a scale-based normalization applied to these data. Figure 5(a) shows the raw spectra and Figure 5(b) shows six different SBN transformations: $\tilde{S}_{k,J}$, for $k = 3, 5$ and $J = 5, 7, 9$. In each case the plots are superimposed on the SVN transformations of these spectra. Note that $\tilde{S}_{3,9}$ and $\tilde{S}_{5,9}$ essentially reproduce the SVN transformation. Indeed, these are close approximations to $\tilde{S}_{1,9} = \tilde{S}_{SNV}$ since the raw spectra are relatively smooth and contain little scale-1 through scale-4 content. At the finest scales, as in $\tilde{S}_{3,5}$, subtle local features are magnified, whereas a focus on midrange scales via $\tilde{S}_{3,7}$ or $\tilde{S}_{5,7}$ produces both a resolution enhancement and a tight agreement in this set of spectra.

4.3 MALDI-TOF spectra

Five MALDI mass spectrometry spectra from the same biological sample that were obtained during a dilution experiment [13] are graphed in Figure 6 after being normalized in

[1] www.idrc-chambersburg.org/shootout_2002.htm

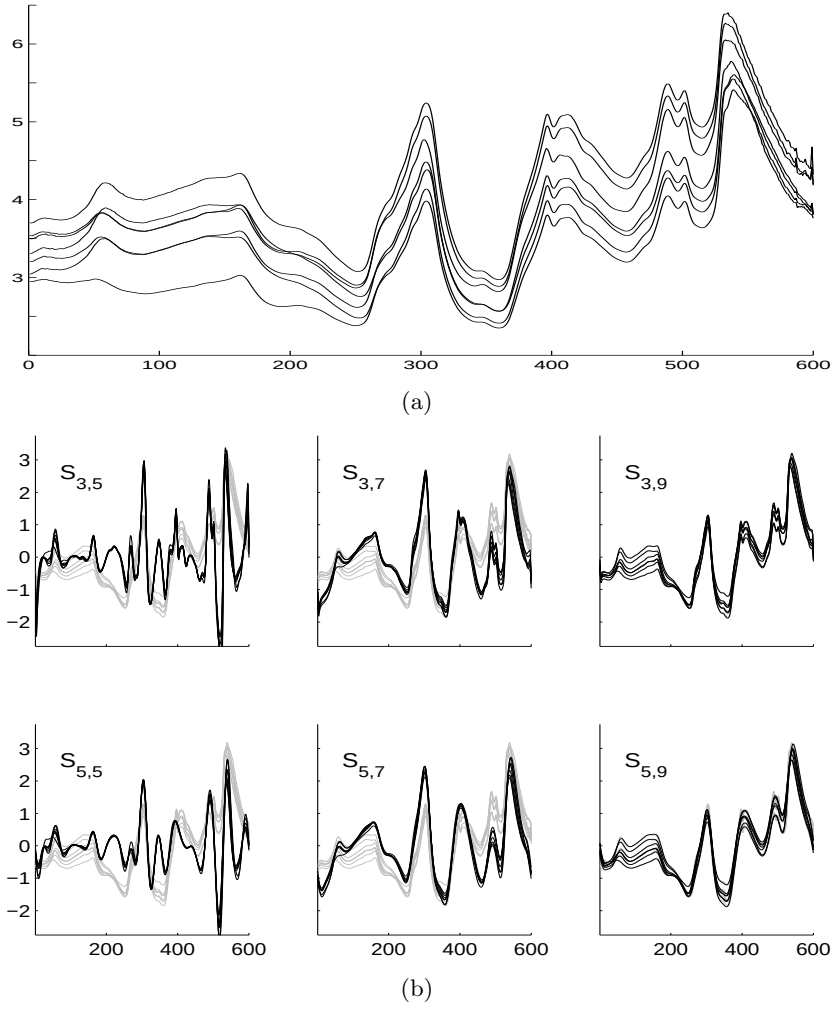

Figure 5: (a) Seven NIR raw spectra. (b) Six different versions of these spectra as transformed by SBN: $\tilde{S}_{k,J}$, for $k = 3, 5$ and $J = 5, 7, 9$. In each subfigure, the $\tilde{S}_{k,J}$ (shown in black) are superimposed on the SNV transformations (gray) of the spectra in (a).

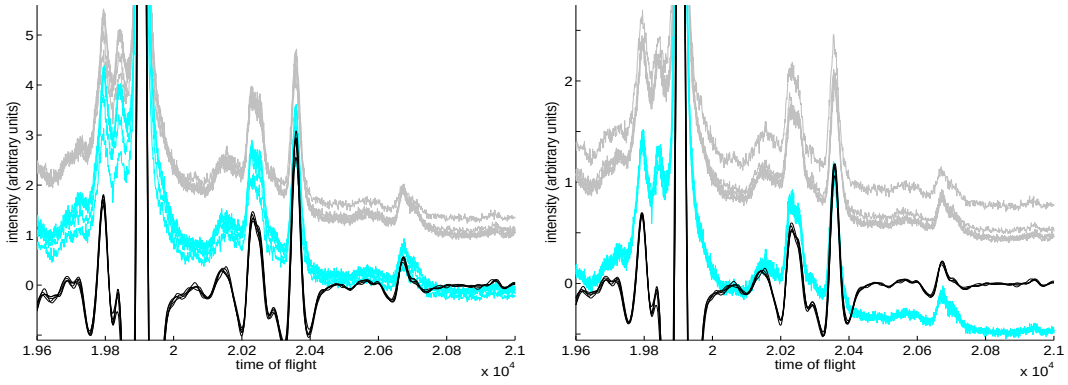

(a) (b)

Figure 6: Replicate MALDI spectra normalized by total energy scaling (gray), SNV (light blue), SBN with $k = 5$ and $J = 6$ (black). In (a) the normalizations are based on all 50,000 TOF measurements and in (b) on the region from 17,000 to 22,000 TOF.

a variety of ways. Only a small portion of these spectra is shown—time-of-flight (TOF) measurements between $19,600$ and $21,000$. In Figure 6(a), the normalizations were performed using all $50,000$ TOF measurements, and in Figure 6(b), a restricted region of $5,000$ TOF measurements (from $17,000$ to $22,000$) was used. In each figure, normalizations from total-energy (gray), SNV (light blue) and SBN with $k = 5,\ J = 6$ (black) are shown.

5 Discussion

The scale-based normalization introduced here provides a generalization of the common SNV approach to normalization of spectral data. By using a multiscale decomposition of each spectrum this approach is less rigidly tied to global variance, baseline trend or high-frequency noise. Flexibility is implemented by restricting the scales of content extracted from each spectrum. Indeed, the SBN approach allows one to bypass high-frequency noise, wide-scale background and/or global trend without explicitly modelling any of these. By including all scales of signal content, the SBN transformation is equivalent to the SNV transformation: $\tilde{S}_{k,J} = \tilde{S}_{SNV}$, for $k = 1, J = \log_2 n$. Although this flexibility introduces greater subjectivity into the normalization process there is no universally unbiased

method that optimally adjusts for all manners in which variation enters the data; careful experimental design and exploratory study of signal content is required in this and every normalization process.

Extracting individual scales of content is implemented through a wavelet multiscale decomposition. Since a wavelet transform acts as differential operator, an added benefit is the potential resolution enhancement obtained by extracting derivative information without the need to first smooth each spectrum. This is particularly important when the raw spectra contain high-frequency noise since the use of derivatives, though common in the analysis of spectral data, is primarily limited to relatively smooth spectra due to the potential instability of numerical differentiation procedures.

Examples from three types of instrumentation illustrate some of the properties of a scale-based normalization. Simulating a variety of random backgrounds in a large set of Raman spectra, the first example contrasts the SNV transformation with its scale-restricted cousin, SBN. Using a set of NIR spectra, a second example exhibits the results from of a wide range of SBN transformations. Finally, a set of MALDI mass spectrometry spectra, each having 50,000 intensity measurements illustrates the robustness of SBN with respect to global properties in the data.

Acknowledgements

This research was financially supported by National Institutes of Health grant GM67211. Additional support from CA086368 is gratefully acknowledged.

References

[1] B. R. Bakshi, *Multiscale analysis and modeling using wavelets*, Journal of Chemometrics **13** (1999), 415–434.

[2] R. J. Barnes, M. S. Dhanoa, and S. Lister, *Standard normal variate transformation and de-trending of near-infrared diffuse reflectance spectra*, Applied Spectroscopy **43** (1989), no. 5, 772–777.

[3] M. Blanco, J. Coello, H. Iturriaga, S. Maspoch, and C. D. L. Pezuela, *Effect of data preprocessing methods in near-infrared diffuse reflectance spectroscopy for the determination of the active compound in a pharmaceutical preparation*, Applied Spectroscopy **51** (1997), no. 2, 240–246.

[4] T. T. Cai, D. Zhang, and D. Ben-Amotz, *Enhanced chemical classification of raman images using multiresolution wavelet transformation*, Applied Spectroscopy **55** (2001), no. 9, 1124–1130.

[5] A. Candolfi, R. De Maesschalck, D. Jouan-Rimbaud, P. A. Hailey, and D. L. Massart, *The influence of data pre-processing in the pattern recognition of excipients near-infrared spectra*, Journal of Pharmaceutical and Biomedical Analysis **21** (1999), 115–132.

[6] P. Geladi, D. MacDougall, and H. Martens, *Linearization and scatter-correction for near-infrared reflectance spectra of meat*, Applied Spectroscopy **39** (1985).

[7] R. S. Gurjar, V. Backman, L. T. Perelman, I. Georgakoudi, K. Badizadegan, I. Itzkan, and R. Dasari M. S. Feld, *Imaging human epithelial properties with polarized lightscattering spectroscopy*, Nature Medicine **7** (2001), no. 11, 1245–1248.

[8] I. S. Helland, T. Naes, and T. Isaksson, *Related versions of the multiplicative scatter correction method for preprocessing spectroscopic data*, Chemometrics and Intelligent Laboratory Systems **29** (1995), 233–241.

[9] M. MacRae, *Rays of hope: Spectroscopy as an emerging tool for cancer diagnostics and monitoring*, Spectroscopy **18** (2003), no. 10, 14–19.

[10] H. Mark and J. Workman, *Derivatives in spectroscopy, Part III–computing the derivative*, Spectroscopy **18** (2003), no. 4, 106–111.

[11] D. B. Percival and A. T. Walden, *Wavelet methods for time series analysis*, Cambridge University Press, Cambridge, UK, 2000.

[12] W. H. Press, S. A. Teukolsky, W. T. Vetterling, and B. P. Flannery, *Numerical recipes in c, the art of scientific computing, 2nd ed.*, Cambridge University Press, Cambridge, UK, 1992.

[13] T. Randolph, B. Mitchell, D. McLerran, P. Lampe, and Z. Feng, *Quantifying peptide signal in MALDI-TOF mass spectrometry data*, Molecular and Cellular Proteomics (2005), in press.

[14] P. Sajda, A. Laine, and Y. Zeevi, *Multi-resolution and wavelet representations for identifying signatures of disease*, Disease Markers **18** (2002), no. 5–6, 339–363.

[15] A. Savitzky and M.J.E. Golay, *Smoothing and differentiation of data by simplified least squares pro,cedures*, Analytical Chemistry **36** (1964), 1627–1639.

[16] N. Sundararajana, D. Mao, S. Chan, T-W. Koo, X. Su, L. Sun, J. Zhang, K b. Sung, M. Yamakawa, P. R. Gafken, T. Randolph, D. McLerran, Z. Feng, A. A. Berlin, and M. B. Roth, *Ultra-sensitive detection and analysis of post-translational modifications using surface enhanced raman spectroscopy (SERS)*, (2005), submitted.

[17] H.-W. Tan and S. D. Brown, *Wavelet analysis applied to removing non-constant, varying spectroscopic background in multivariate calibration*, Journal of Chemometrics **16** (2002), 228–240.

[18] M. Zeaiter, J.-M. Roger, and V. Bellon-Maurel, *Robustness of models developed by multivariate calibration. Part II: The influence of pre-processing methods*, Trends in Analytical Chemistry **24** (2005), no. 5, 437–445.

[19] D. Zhang and D. Ben-Amotz, *Enhanced chemical classification of raman images in the presence of strong fluorescence interference*, Applied Spectroscopy **54** (2000), no. 9, 1379–1383.